Original Article

Early SUV_{max} is the best predictor of axillary lymph node metastasis in stage III breast cancers

Jiangong Zhang[1,2], Xun Shi[2], Yong Xiao[3], Chao Ma[4], Gang Cao[5], Yongbo Liu[5#], Yonggang Li[1#]

[1]Department of Radiology, The First Affiliated Hospital of Soochow University, Suzhou, China; [2]Department of Nuclear Medicine, The First People's Hospital of Yancheng, The Fourth Affiliated Hospital of Nantong University, Yancheng, China; [3]Department of MRI Room, The First People's Hospital of Yancheng, The Fourth Affiliated Hospital of Nantong University, Yancheng, China; [4]Department of Nuclear Medicine, Tenth People's Hospital of Tongji University, Shanghai, China; [5]Department of Radiology, Peking University Lu'an Hospital, Changzhi, China

[#]These authors contributed equally to this work.

Correspondence to: Yongbo Liu, MD. Department of Radiology, Peking University Lu'an Hospital, Changzhi, China. Email: lyb126ct@126.com; Yonggang Li, MD. Department of Radiology, The First Affiliated Hospital of Soochow University, Suzhou, China. Email: Liyonggang2020@126.com.

Background: Although fluorine-18-labeled 2-fluoro-2-deoxy-D-glucose (^{18}F-FDG) positron emission/computed tomography (PET/CT) imaging has been investigated for its ability to evaluate lymph node metastasis of breast cancer, few comparative analyses have evaluated the preoperative and postoperative regional lymph node metastasis of breast cancer by dual-phase imaging, especially in patients with stage III (N2) disease.

Methods: The clinical, pathological, and imaging data of 40 patients with stage III (N2) breast cancer were retrospectively analyzed. All patients underwent dual-time point ^{18}F-FDG imaging before surgery and postoperative pathology examinations were obtained. The short-axis lymph node diameter was measured, and the maximum standardized uptake value (SUV_{max}) and the percentage difference of SUV_{max} between dual-phase (ΔSUV_{max}) were calculated to compare metastatic and non-metastatic lymph nodes on dual-time point images.

Results: A total of 398 axillary lymph nodes were inspected, and 209 lymph nodes were matched with those on PET/CT images, including 97 metastatic and 112 non-metastatic lymph nodes. The SUV_{max} values were significantly different between metastatic and non-metastatic lymph nodes, in both the early and delayed scans (P<0.001). For metastatic lymph nodes, the SUV_{max} value on the delayed scan (6.17±2.62) was significantly higher compared with the early scan (5.45±1.35; ΔSUV_{max} =0.08±0.21, P<0.001). Moreover, the SUV_{max} values were not significantly different between the delayed (2.82±0.91) and early scans (2.79±0.72; ΔSUV_{max}=−0.00±0.11, P=0.77). The short diameters were not significantly different between metastatic and non-metastatic lymph nodes (P=0.12), and the SUV_{max} values of metastatic lymph nodes with short diameters of >4.00 and ≤6.00 mm were not significantly different between the early and delayed scans (P=0.06). However, the SUV_{max} values of metastatic lymph nodes with short diameters of >6.00 and ≤8.00 mm (7.11±0.19 *vs.* 5.96±0.08) and short diameters of >8.00 and ≤10.00 mm (10.76±0.35 *vs.* 6.82±0.50) were higher on the delayed scan versus the early scan, respectively (P<0.01 for each comparison). The difference between the ΔSUV_{max} values among the three subgroups was statistically significant (F=78.98, P<0.001). The receiver operating characteristic (ROC) curve analysis of the lymph nodes showed that the area under the curve (AUC) of the early and delayed PET/CT scans was 0.961 (0.925–0.983, P=0.013) and 0.897 (0.847–0.934, P=0.022), respectively. The ROC curves of the early and delayed scans were also significantly different (z=4.46, P<0.001). AUC of the ΔSUV_{max} for the early scan was significantly lower compared with delayed scans (z=8.95 *vs.* 9.13, respectively; P<0.001).

Conclusions: Dual-time point ^{18}F-FDG PET imaging significantly improved the prediction and detection of axillary lymph node metastasis, compared with prediction based on size of lymph node alone, in patients with stage III breast cancer. We found that lymph nodes with continuously increased SUV_{max} values tended to show

metastasis, and early SUV_{max} assessment offers the best capacity for prediction of axillary lymph node metastasis.

Keywords: Breast neoplasms; lymph nodes; positron emission tomography (PET); fluorine-18-labeled 2-fluoro-2-deoxy-D-glucose (^{18}F-FDG); maximum standardized uptake value (SUV_{max})

Submitted Mar 11, 2020. Accepted for publication Nov 13, 2020.
doi: 10.21037/qims-20-423
View this article at: http://dx.doi.org/10.21037/qims-20-423

Introduction

Breast cancer is the most common malignant tumor in women worldwide (1,2), and the incidence of breast cancer is increasing each year in China (3,4). Lymphatic metastasis is the most common type of metastasis (5,6), and the axillary lymph node is the first site of breast cancer metastasis, which compresses the axillary vein and results in edema of the upper limb on the affected side. Edema then extends to the clavicle and the internal mammary lymph node, which leads to metastasis of the lung, pleura, bone, liver, brain, kidney and other areas, and may result in direct invasion of the surrounding tissue of the chest wall. Moreover, different pathological types of metastasis vary in associated symptoms and signs. As breast cancer progresses, deterioration occurs. The later the disease progression, the greater the possibility of systemic metastasis and the more difficult it is to treat. Recalcitrant disease is associated with reduced patient quality of life and increased mortality. Regional lymph node metastasis plays an important role in treatment planning and prognosis prediction. Axillary lymph node dissection (ALND) is a routine, but highly invasive surgery to determine the lymph node stage of breast cancer. Recently, sentinel lymph node biopsy (SLNB) has been developed, through which ALND can be avoided if the sentinel lymph node is negative. However, surgical trauma is still associated with SLNB, and traditional imaging methods, such as ultrasonography, magnetic resonance imaging (MRI), and computed tomography (CT) have limited effectiveness in evaluating lymph node metastasis (7,8).

Positron emission tomography (PET) is a kind of imaging technology that displays biological activity *in vivo*, at the molecular level. PET mainly uses fluorine-18 (^{18}F) and other positron nuclides to label various biomolecules. This labeling allows the biological characteristics and functions of the marker molecules to remain intact, while permitting objective display of biological processes *in vivo*, revealing genetic, metabolic, and functional changes that are occurring due to the disease, and providing a scientific basis for early detection. Because of the high sensitivity and specificity of PET, this imaging method provides the possibility for non-invasive diagnosis of breast cancer and axillary lymph node metastasis, providing a basis for treatment selection and allowing dynamic observation of response to treatment. Although fluorine-18-labeled 2-fluoro-2-deoxy-D-glucose positron emission tomography and computed tomography (^{18}F-FDG PET/CT) imaging has been used in the study of lymph node metastasis in breast cancer (9-11), dual-time imaging studies in this area are still rare.

The axillary lymph node is the first site of breast cancer metastasis, and early detection of metastasis to this site is critical. Therefore, we retrospectively analyzed dual-phase ^{18}F-FDG PET/CT imaging findings, in which the change in SUV_{max} values was calculated and compared between metastatic and non-metastatic lymph nodes, as well as among subgroups of metastatic lymph nodes. Furthermore, differences in SUV_{max} values were evaluated for predictive capacity in the preoperative detection of axillary lymph node metastasis in patients with stage III breast cancer.

Methods

Participants

Clinical data from 40 women with breast cancer who underwent ^{18}F-FDG PET/CT examinations from December 2016 to December 2019 in our hospital were retrospectively analyzed (Table S1). All patients had the following characteristics: unilateral lesions without distant metastasis; no second primary tumor; no cancer-related treatment; no current pregnancy or lactation; and dual-phase PET/CT imaging 1–2 weeks before surgery. The patients were divided into two groups based on their average age (55.6 years, ranged from 33 to 72 years) for further analysis. According to histopathological assessment, all 40 patients had stage III (N2) disease, including 31 patients with invasive ductal carcinoma and 9 patients with invasive

lobular carcinoma. Patients were divided into two groups according to the average diameter of tumor (2.58 cm, ranged from 0.8 to 5.7 cm) for further analysis. A total of 398 axillary lymph nodes were resected, including 176 metastatic lymph nodes and 222 non-metastatic lymph nodes. A total of 209 lymph nodes were matched with the lymph nodes on PET/CT images, including 97 metastatic lymph nodes and 112 non-metastatic lymph nodes. Ethical approval was obtained from the institutional review boards and the requirement of informed consent was waived due to the retrospective nature of this study.

Dual-time point ^{18}F-FDG PET/CT imaging

The ^{18}F-FDG was provided by Shanghai Atomic Kexing Pharmaceutical Co., Ltd., China. The PET/CT imaging instrument was a 64-slice Siemens Biograph mCT with a ring consisting of 52 detectors. The patients fasted for at least 4–6 h and had a fasting blood sugar level of 4.0–8.2 mmol/L. After an intravenous injection of ^{18}F-FDG at a dose of 4.81 MBq/kg body mass, the patients were instructed to lie down in the dark for 60–70 min. The bladder was emptied before the early scan, which ranged from the skull base to the middle of the upper femur. Plain CT scan was performed, first with a current of 170 mA, voltage of 120 kV, scanning time of 18.66–21.94 s, pitch of 0.8, rotational speed of 0.5 s/rot and scanning thickness of 3 mm and then a PET scan, a total of 6–7 body positions (via changing the bed position) were imaged at a scanning rate of 2 min/position (early SUV_{max}). The bladder was emptied again 120 to 150 min after FDG injection, delayed scan was acquired at a scanning rate of 4 min/position (delayed SUV_{max}), ranging from the skull base to the middle of the upper femur (6–7 body positions). The images were reconstructed after attenuation correction, and fusion images of the transverse, coronal, and sagittal views of PET, CT, and PET/CT scans with 5 mm thickness were obtained.

Image analysis

The PET/CT images were assessed by two experienced radiologists. A region of interest (ROI) was used to determine the maximum standardized uptake value (SUV_{max}) of the matched lymph nodes on the PET/CT fusion images, and the SUV_{max} values at the early and delayed stages were calculated accordingly. The change in SUV_{max} was determined using the following equation:

Delta SUV_{max} (ΔSUV_{max}) = (delayed SUV_{max}– early SUV_{max})/early SUV_{max}

The short-axis lymph node diameters were measured on plain CT sections. There was a limitation on scanning thickness and it was difficult to accurately delineate the ROIs, therefore lymph nodes with a short-axis diameter of less than 4 mm were excluded. During the operation, the matched lymph nodes on PET/CT were located and labeled according to the lymph node size, shape, direction, and the distance from the primary breast cancer. The lymph nodes were identified as metastatic lymph nodes by optical microscopy.

Statistical analysis

Data were analyzed using SPSS 20.0 and MedCalc 12.7 software. Continuous data were expressed as mean ± standard deviation. Correlation of lymph nodes with clinicopathological parameters was assessed using the χ^2 test. One-way ANOVA was used to compare subgroups of metastatic lymph nodes. Comparison between groups was performed using the two-sample *t*-test or the paired t-test. The diagnostic efficacy and diagnostic threshold in three types of values (early, delayed phases and Delta SUV_{max}) were analyzed using receiver operating characteristic (ROC) curves, and ROC curves between every two types were compared using the Delong test. $P<0.05$ was considered statistically significant.

Results

Clinical characteristics of the patients

In the resected lymph nodes, metastasis and non-metastasis were not related to age, pathological type, location, molecular subtype, Scarff-Bloom-Richardson (SBR), or size of primary focus (P values were 0.534, 0.595, 0.496, 0.524, 0.525 and 0.658, respectively). The matching of lymph nodes with PET/CT data showed no correlation with clinical characteristics (P values were 0.260, 0.765, 0.532, 0.788, 0.883 and 0.516, respectively). The short-axis diameters were not significantly different between the metastatic and non-metastatic lymph nodes ($t=1.56$, $P=0.121$). The SUV_{max} values for contralateral normal axillary region on the delayed scans were not significantly higher compared with the early scans ($t=1.65$, $P=0.107$). The SUV_{max} values for tumors on the delayed scans were significantly higher compared with the early scans ($t=25.89$, $P<0.001$; *Table 1*) (*Figures 1,2*). There was no

Table 1 Clinical characteristics of the patients

Variables	Number of cases	Total number of lymph nodes (n=398)			Matched lymph nodes (n=209)		
		MLN	NMLN	P*	MLN	NMLN	P**
Age (years)				0.534			0.260
≤55	19	80	94		50	49	
>55	21	96	128		47	63	
Tumor site				0.496			0.532
Left breast	22	98	116		57	61	
Right breast	18	78	106		40	51	
Pathological types				0.595			0.765
Invasive ductal carcinoma	31	134	174		77	87	
Invasive lobular carcinoma	9	42	48		20	25	
Molecular subtype				0.524			0.788
Luminal A	21	86	117		48	57	
Luminal B	10	43	59		21	29	
HER2 (+)	4	24	21		15	14	
TNBC	5	23	25		13	12	
Scarff-Bloom-Richardson				0.595			0.883
I	16	64	89		35	43	
II	13	60	77		34	40	
III	11	52	56		28	29	
Tumor diameter (cm)				0.658			0.516
≤2.5	19	84	101		52	55	
>2.5	21	92	121		45	57	
Short diameters (mean ± SD)					6.25±1.25	6.02±0.79	0.121
SUV_{max} of tumor (mean ± SD)							
Early phase	6.82±0.50						
Delayed phase	9.05±0.91$^{\triangle}$						
SUV_{max} of CNAR (mean ± SD)							
Early phase	0.283±0.048						
Delayed phase	0.279±0.043$^{\triangledown}$						
ΔSUV_{max}	−0.012±0.044						

P* correlation with variables in total number of lymph nodes; P** correlation with variables in matched lymph nodes matched with PET/CT. $^{\triangle}$Compared with early stage, t=25.89, P<0.001; $^{\triangledown}$Compared with early stage, t=1.65, P=0.107. MLN, metastatic lymph nodes; NMLN, non-metastatic lymph nodes; HER2, human epidermal growth factor receptor 2; TNBC, triple-negative breast cancer; CNAR, contralateral normal axillary region; SUV_{max}, maximum standardized uptake value.

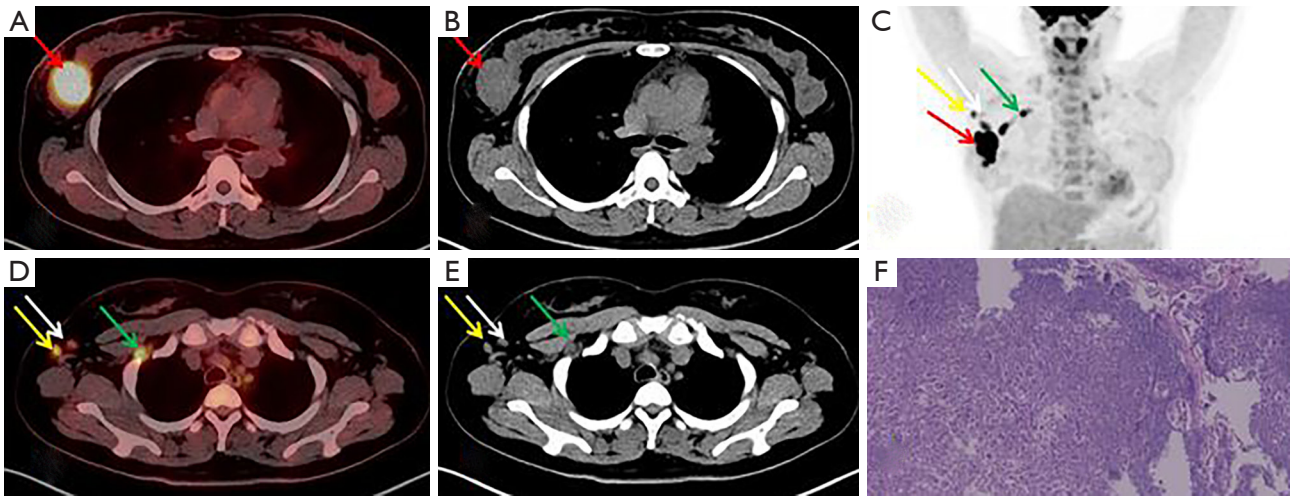

Figure 1 ^{18}F-FDG PET/CT imaging and pathology of right breast outer upper quadrant invasive ductal carcinoma (A-F, female, 37 years old). Red arrow shows primary breast cancer. White arrow shows that the short diameter of lymph node is 6.35 mm, the SUV_{max} values on the early scan (1.58) and delayed scan (1.65), but no metastasis is found in postoperative pathology. Yellow arrow shows that the short diameter of lymph node is 6.51 mm, the SUV_{max} values on the early scan (4.21) and delayed scan (4.87). Green arrow shows that the short diameter of lymph node is 7.23 mm, the SUV_{max} values on the early scan (6.56) and delayed scan (7.98). These two lymph nodes can be seen with pathological metastasis after operation (F, HE×10).

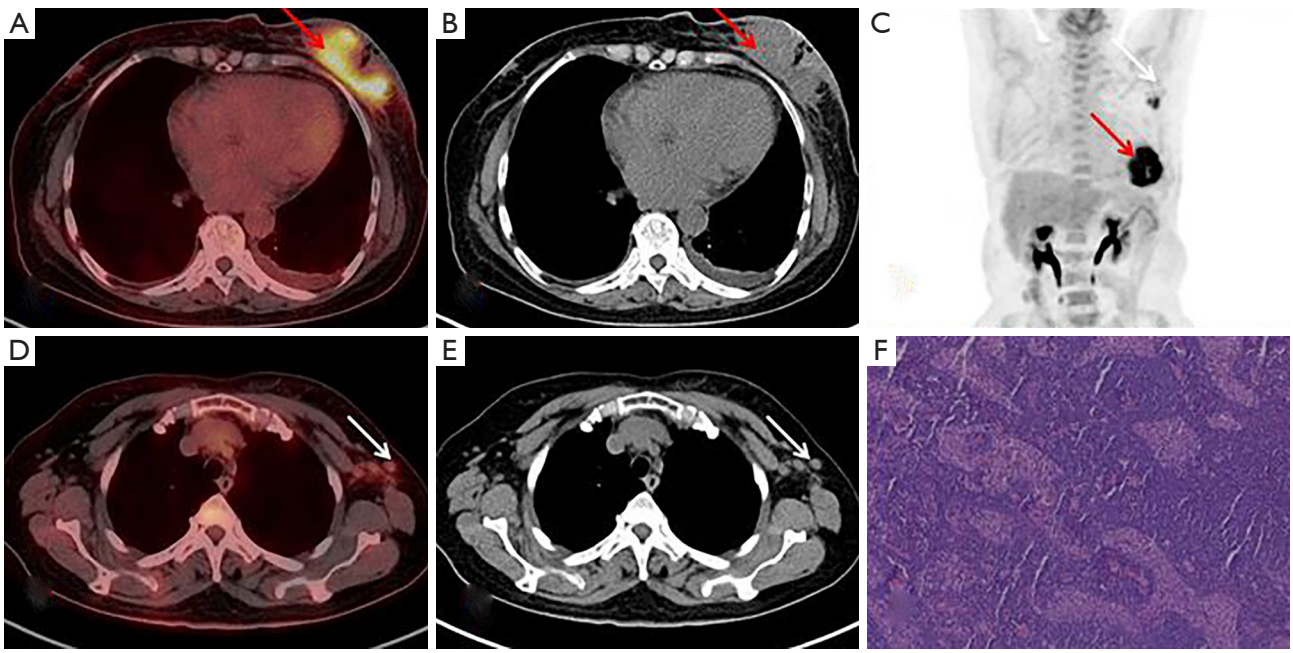

Figure 2 ^{18}F-FDG PET/CT imaging and pathology of left breast invasive ductal carcinoma (A-F, female, 71 years old). Red arrow shows primary breast cancer. White arrow shows that the short diameter of lymph node is 6.03 mm, the SUV_{max} values on the early scan (1.51) and delayed scan (1.59), but no metastasis is found in postoperative pathology (F, HE×10).

Table 2 Comparison of the dual-phase SUV_{max} values in histologic subtypes of matched metastatic lymph nodes

Variables	Number of MLN	Early phase	P	Delayed phase	P
Pathological types					
Invasive ductal carcinoma	77	5.597±1.427	0.164	6.258±2.846	0.565
Invasive lobular carcinoma	20	5.126±0.910		5.877±1.473	
Scarff-Bloom-Richardson					
I	35	4.552±1.135	<0.001	4.753±1.883	<0.001
II	34	5.528±0.985		6.102±2.485	
III	28	6.651±1.047		8.055±2.470	

MLN, metastatic lymph nodes; SUV_{max}, maximum standardized uptake value.

Table 3 Comparison of the SUV_{max} values of dual-phase images between the metastatic and non-metastatic group in matched lymph nodes

SUV_{max}	Metastasis (n=97)	Non-metastatic (n=112)	t	P
Early phase	5.45±1.35	2.79±0.72	17.78	<0.001
Delayed phase	6.17±2.62*	2.82±0.91**	12.01	<0.001
ΔSUV_{max}	0.08±0.21	−0.00±0.11	3.46	0.001

*Compared with early stage, t=−4.96, P<0.001; **Compared with early stage, t=−0.30, P=0.766; SUV_{max}, maximum standardized uptake value; ΔSUV_{max} = (delayed SUV_{max} − early SUV_{max})/early SUV_{max}.

significant difference in SUV_{max} of the early and delayed phases between the invasive ductal carcinoma and invasive lobular carcinoma (t=1.40 and 0.58, P =0.164 and 0.565, respectively). However, we analyzed the I, II and III grades of SBR, and found that the worse the degree of differentiation, the greater the SUV_{max}, and the difference was statistically significant (F=30.57 and 16.33, respectively, P<0.001; *Table 2*).

Comparison of the SUV_{max} of metastatic and non-metastatic lymph nodes

The SUV_{max} of metastatic lymph nodes from the delayed scan images was significantly higher compared with the early scan images (t=−4.96, P<0.001), and the ΔSUV_{max} on the dual-phase images was 0.08±0.21. The SUV_{max} value of non-metastatic lymph nodes from the delayed scan images was higher compared with the early scan images (t=−0.30, P=0.766). *Table 3* reveals that the SUV_{max} values from the early and delayed scan images were each significantly different between the metastatic and non-metastatic lymph nodes (P<0.001) (*Figure 3*).

Comparison SUV_{max} in metastatic lymph node subgroups

The SUV_{max} values were not significantly different in the subgroup with short diameters of >4.00 and ≤6.00 mm when comparing early and delayed scans (t=1.96, P=0.06). The SUV_{max} value from the delayed scan was higher compared with the early scan in the subgroup with short diameters of >6.00 and ≤8.00 mm, as well as in the subgroup with short diameters of >8.00 and ≤10.00 mm; both of these differences were significant (t=9.67 and 17.34, respectively, P<0.001; *Table 4*).

Comparison of the change in SUV_{max}

The ΔSUV_{max} values were significantly different between metastatic and non-metastatic lymph nodes (t=3.46, P=0.001; *Table 3*). The differences in ΔSUV_{max} values among the three metastatic subgroups (4.00mm< short diameter ≤6.00 mm, 6.00 mm < short diameter ≤8.00 mm and 8.00 mm < short diameter ≤10.00 mm) were statistically significant (F=78.98, P<0.001), and the differences between every two subgroups were statistically significant (P<0.001; *Table 4*).

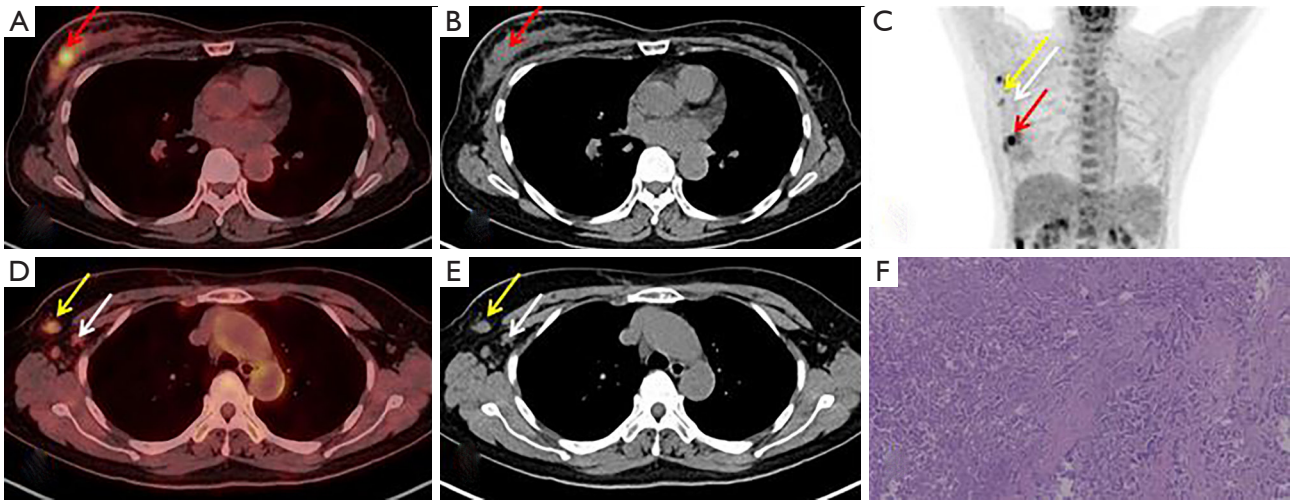

Figure 3 ^{18}F-FDG PET/CT image of another patient with invasive ductal carcinoma of the right upper outer quadrant of the breast (A-F, female, 53 years old). Red arrow shows primary breast cancer. White arrow shows that the short diameter of lymph node is 5.45 mm, the SUV_{max} values on the early (1.43) and delayed scan (1.51), and no metastasis is found in postoperative pathology. Yellow arrow shows that the short diameter of lymph node is 6.56 mm, the SUV_{max} values on the early scan (3.82) and delayed scan (4.49), but metastasis is found in postoperative pathology (F, HE×10).

Table 4 Comparison of the dual-phase SUV_{max} values in subgroups of matched metastatic lymph nodes

SUV_{max}	4.00< short diameter ≤6.00 mm (n=43)	6.00< short diameter ≤8.00 mm (n=45)	8.00< short diameter ≤10.00 mm (n=9)
Early phase	4.55±0.19	5.96±0.08	7.75±0.19
Delayed phase	4.25±0.32	7.11±0.19	10.76±0.35
T	1.96	9.67	17.34
P	0.056	<0.001	<0.001
ΔSUV_{max}	−0.10±0.15	0.18±0.12	0.39±0.05

SUV_{max}, maximum standardized uptake value; ΔSUV_{max} = (delayed SUV_{max} − early SUV_{max})/early SUV_{max}.

Analysis and comparison of ROC curves

ROC curve analysis showed that the AUC of SUV_{max} in the early phase was 0.961 (P=0.013, 95% CI: 0.925–0.983), and the diagnostic threshold was 4.29. The sensitivity and specificity for diagnosing metastatic lymph nodes were 82.5% and 100%, respectively. The AUC of SUV_{max} in the delayed phase was 0.897 (P=0.022, 95% CI: 0.847–0.934), and the diagnostic threshold was 4.33. The sensitivity and specificity for diagnosing metastatic lymph nodes were 73.2% and 100%, respectively. The AUC of the ΔSUV_{max} was 0.602 (P=0.043, 95% CI: 0.532–0.669), and the diagnostic threshold was 0.18. The sensitivity and specificity for diagnosing metastatic lymph nodes were 39.2% and 100%, respectively (*Table 5*, *Figure 4*).

The sensitivities in the delayed phase and ΔSUV_{max} were lower than that in the early phase. The difference of AUC between the early and delayed phases was statistically significant (z=4.46, P<0.001). Furthermore, the AUC of ΔSUV_{max} was significantly lower than the early and delayed scans (z=8.95 and 9.13, respectively, P<0.001) (*Table 6*).

Discussion

Breast cancer cells are prone to shedding into the lymphatic system or blood, leading to metastasis and posing a greater risk of death (12). The lymphatic system is one of the most common routes of cancer cell dispersal; therefore, lymph node metastasis plays a critical role in staging, treatment planning, and establishing a prognosis for breast cancer

Table 5 Analysis of ROC curves for three types of values

Phases	Sensitivity	Specificity	AUC	P	Threshold	95% CI
Early phase	82.5%	100%	0.961	0.013	4.29	0.925–0.983
Delayed phase	73.2%	100%	0.897	0.022	4.33	0.847–0.934
ΔSUV_{max}	39.2%	100%	0.602	0.043	0.18	0.532–0.669

ROC, receiver operating characteristic; AUC, area under curve; IC, confidence interval.

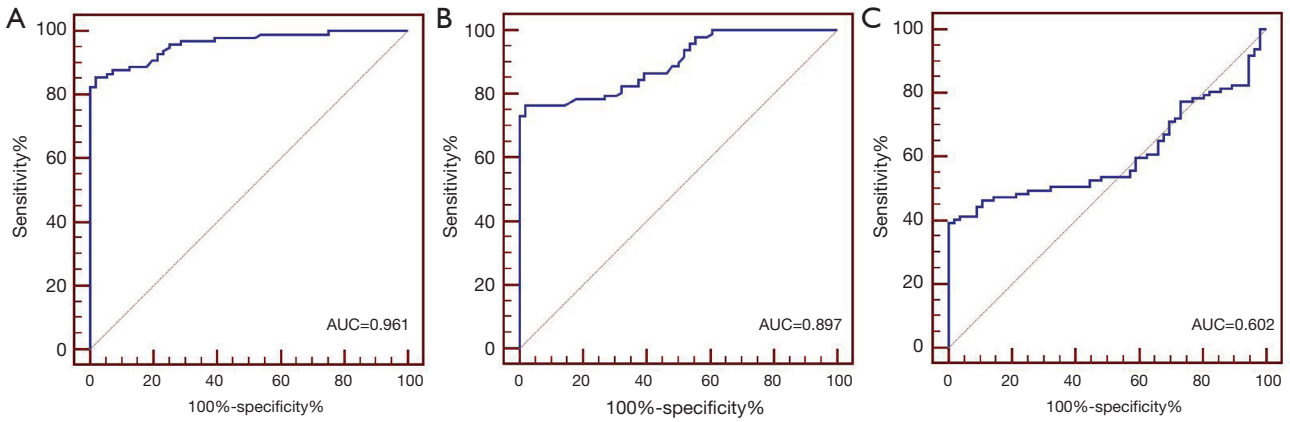

Figure 4 ROC curve of the SUV_{max} and ΔSUV_{max} values on dual-phase images for diagnosing metastatic lymph nodes. The sensitivity in delayed phase and ΔSUV_{max} were lower than that in early phase. (A) AUC of early phase was 0.961; (B) AUC of delayed phase was 0.897; (C) AUC of ΔSUV_{max} was 0.602.

Table 6 Comparison of ROC curves between every two types of values

Phases	z	P*
Early and Delayed phase	4.46	<0.001
Early phase and ΔSUV_{max}	8.95	<0.001
Delayed and ΔSUV_{max}	9.13	<0.001

*Delong test between every two types of values.

(13-15). With improvements in the diagnosis and treatment of breast cancer, there is an urgent need to, clarify the stage of breast cancer accurately and effectively by evaluating lymph node metastasis. Traditional imaging methods, such as CT, MRI, and ultrasonography, play a role in evaluating axillary lymph node morphology (16). However, small or irregular lymph node metastases can be easily overlooked when using these methods during diagnosis (17,18). Some studies have shown that ^{18}F-FDG PET/CT detection of lymph node metastasis may allow patients to avoid SLNB (19). The use of ^{18}F-FDG PET/CT in the evaluation of lymph node metastasis in breast cancer has also been described (9,20-24). However, few comparative analyses have assessed the preoperative and postoperative regional lymph node metastasis of breast cancer by dual-phase imaging. In this study, an ROC curve was used to analyze the diagnostic efficacy and determine the optimal SUV_{max} threshold for diagnosing metastatic lymph nodes.

Some studies have found difficulties in the differential diagnosis of some inflammatory or infectious lesions and malignant lesions with PET/CT dual-phase imaging (25). Other studies have suggested that the FDG uptake in tumor cells increases over time, while mononuclear uptake due to inflammation and other major factors decreases over time (26). The uptake of ^{18}F-FDG in the lesions may be underestimated by a single imaging around 1 hour after the imaging agent injection. Dual-phase imaging and delayed imaging can improve the diagnostic efficacy in differentiating benign and malignant lesions (27). In the present study, we showed that metastatic lymph nodes had a significantly higher SUV_{max} value on delayed scans compared with early scans, and primary breast cancer had a significantly higher SUV_{max} value on delayed scans compared with early scans as well. Moreover, non-

metastatic lymph nodes had a slightly higher SUV_{max} value on delayed scans compared with early scans, although the difference was not statistically significant. These findings were consistent with the above-mentioned reports. The SUV_{max} values from the delayed and early scans of metastatic lymph nodes were significantly higher compared with the non-metastatic lymph nodes, suggesting that dual-phase and delayed phase imaging could improve visualization of lymph node metastases in breast cancer, which is an outcome of immense diagnostic value. An SUV_{max} that was increased on the delayed image of the lymph node suggested that the lymph node had a tendency towards metastasis, which could be attributed to the uptake peak of ^{18}F-FDG by tumor cells occurring at 3–4 h after injection, whereas the uptake peak of inflammatory lesions occurs at approximately 1 h after injection (28,29).There were also some studies supporting the view that the peak value of SUV_{max} for inflammatory or infectious diseases was longer (30). In this study, early imaging at 60–70 min after the injection captured the peak uptake time of non-metastatic lymph nodes, whereas the SUV_{max} value of non-metastatic lymph nodes was lower compared with the metastatic lymph nodes during the non-peak uptake time. After a 120–150 min delay of imaging, the uptake of ^{18}F-FDG in the tumor cells was still increasing. However, few studies have investigated the diagnostic value of PET/CT in different pathological types of breast cancer at home and abroad (31).

In this study, the SUV_{max} values of metastatic lymph nodes and non-metastatic lymph nodes in patients with breast cancer were 5.45±1.35 and 2.79±0.72, respectively, which were different from those in a previously reported study (32). Such a discrepancy may reflect that the determination of SUV is affected not only by physiological factors, such as patient body weight and blood glucose concentration, but also by the software and hardware involved in imaging and analysis, including acquisition modes of different equipment, attenuation correction methods, and reconstruction algorithms (33,34). Therefore, there may be substantial differences in the SUV_{max} values of benign and malignant tumors determined by various PET centers. Further ROC curve analyses showed that the AUC of early imaging was 0.961, and the sensitivity and specificity of a SUV_{max} >4.29 for diagnosing metastatic lymph nodes were 82.5% and 100%, respectively. The AUC of delayed imaging was 0.897, and the sensitivity and specificity of a SUV_{max} >4.33 for diagnosing metastatic lymph nodes were 73.2% and 100%, respectively. The AUC of the ΔSUV_{max} was 0.602. The difference in AUC between the early and delayed scans was statistically significant (P<0.001), and the AUC of the ΔSUV_{max} was significantly lower for the early compared with the delayed scans (P<0.001), suggesting that the increase in SUVmax upon delayed imaging predicts a tendency towards lymph node metastasis, albeit with decreased sensitivity. Therefore, the early SUV_{max} offers the best value in predicting axillary lymph node metastasis in stage III (N2) breast cancers. The size of SUV_{max} was not only related to the degree of malignancy of the tumor, but also related to the size of the lesion. The metastatic lymph nodes were further divided into three subgroups. The results showed that the SUV_{max} values of some small metastatic lymph nodes (4.00< short diameter ≤6.00 mm) were not significantly increased, and even slightly decreased, between the early and delayed scans. This made the overlap between the SUV_{max} values on the delayed image for non-metastatic lymph nodes wider than that on the early image for non-metastatic lymph nodes. This study suggested that FDG uptake peaks occurred earlier than anticipated in some small metastatic lymph nodes, an effect that may be related to tumor heterogeneity (35), and may contribute to missed diagnoses with both single- and dual-phase imaging for small metastatic lymph nodes. We believe that the smaller the lymph node is, the greater the diagnostic value of SUV_{max} in the early phase, and SUV_{max} in the delayed phase can be used as supplementary diagnostic information. However, some studies suggested that some inflammatory or infectious lesions reduced the diagnostic efficiency of dual phase imaging (36). Therefore, it is necessary to perform further research with larger sample sizes.

Ma *et al.* (37) found that the standard attributes indicating lymph node metastasis were different depending on the sites, e.g., the short-axis diameter of the ipsilateral retropharyngeal lymph node >5 mm, the short diameter of the middle lymph node >11 mm, and the short diameter of other parts >10 mm. Lymph nodes with a short diameter of <1 cm on CT images cannot be excluded from the possibility of metastasis (38). In this study, the average short diameter of 97 metastatic lymph nodes was 6.25±1.25 mm, which was consistent with the results of the above-mentioned studies. The average short diameter of 112 non-metastatic lymph nodes was 6.02±0.79 mm, which was smaller than that of the metastatic lymph nodes, although the difference was not significant. We selected as few cases of stage N2 lymph node metastases as possible and excluded some cases of lymph node fusion or stage N2 metastases to accurately match the preoperative PET/CT findings of lymph nodes with the postoperative pathology, which may

contribute to the lack of significance in diameter variation.

The present study has several limitations. First, the number of cases was relatively small, and all included cases featured high ^{18}F-FDG uptake in the primary lesion, which failed to allow interpretation that accounts for the heterogeneity of pathological types and differentiation. Second, there was selection bias. Some cases of metastases higher than stage N2 or lymph node fusion were excluded during case selection to accurately match the pathological lymph node results with the preoperative PET/CT findings. Third, this was a retrospective study, and although only cases with axillary lymph node metastasis below stage N2 were included, some matching errors may remain. Finally, at present, we still face the problem of low sensitivity of small lesions in the absence of SLNB. Therefore, the differential diagnosis between small metastatic lymph nodes and other lesions should be more cautious.

Conclusions

Lymph node size had limited value in the diagnosis of axillary lymph node metastasis of breast cancer. In contrast, dual-phase ^{18}F-FDGPET/CT imaging had great value in evaluating axillary lymph node metastasis of stage III breast cancer. An SUV_{max} that continuously increased in a lymph node suggested metastasis, and early SUV_{max} offers the best value in predicting axillary lymph node metastasis in stage III breast cancers.

Acknowledgments

Funding: The authors would like to thank the national natural science foundation of China (No. 81671743), clinical key diseases diagnosis and therapy special foundation of Suzhou City (Grant number LCZX201801), and high-level health talent project of Jiangsu Province (Grant number LGY2016035).

Footnote

Conflicts of Interest: All authors have completed the ICMJE uniform disclosure form (available at http://dx.doi.org/10.21037/qims-20-423). The authors have no conflicts of interest to declare.

Ethical Statement: Ethical approval was obtained from the institutional review boards and the requirement of informed consent was waived due to the retrospective nature of this study.

References

1. Zuo TT, Zheng RS, Zeng HM, Zhang SW, Chen WQ. Female breast cancer incidence and mortality in China, 2013. Thorac Cancer 2017;8:214-8.
2. Abubakar M, Sung H, Bcr D, Guida J, Tang TS, Pfeiffer RM, Yang XR. Breast cancer risk factors, survival and recurrence, and tumor molecular subtype: analysis of 3012 women from an indigenous Asian population. Breast Cancer Res 2018;20:114.
3. Shi XJ, Au WW, Wu KS, Chen LX, Lin K. Mortality characteristics and prediction of female breast cancer in China from 1991 to 2011. Asian Pac J Cancer Prev 2014;15:2785-91.
4. Yan X, Han R, Zhou J,Yu H, Wu M. Incidence, mortality and survival of female breast cancer during 2003-2011 in Jiangsu province, China. Chin J Cancer Res 2016;28:321-9.
5. Nathanson SD, Krag D, Kuerer HM, Newman LA, Brown M, Kerjaschki D, Pereira ER, Padera TP. Breast cancer metastasis through the lympho-vascular system. Clin Exp Metastasis 2018;35:443-54.
6. Yu X, Hao X, Wan J, Wan J, Yu L, Liu B. Correlation between Ultrasound Appearance of Small Breast Cancer and Axillary Lymph Node Metastasis. Ultrasound Med Biol 2018;44:342-9.
7. Hao Y, Ren G, Yang W, Zheng W, Wu Y, Li W, Li X, Li Y, Guo X. Combination diagnosis with elastography strain ratio and molecular markers effectively improves the diagnosis rate of small breast cancer and lymph node metastasis. Quant Imaging Med Surg 2020;10:678-91.
8. Wen X, Yu X, Tian Y, Liu Z, Cheng W, Li H, Kang J, Wei T, Yuan S, Tian J. Quantitative shear wave elastography in primary invasive breast cancers, based on collagen-S100A4 pathology, indicates axillary lymph node metastasis. Quant Imaging Med Surg 2020;10:624-33.
9. Yararbas U, Avci NC, Yeniay L, Argon AM. The value

of 18F-FDG PET/CT imaging in breast cancer staging. Bosn J Basic Med Sci 2018;18:72-9.
10. Song BI, Kim HW, Won KS. Predictive Value of 18F-FDG PET/CT for Axillary Lymph Node Metastasis in Invasive Ductal Breast Cancer. Ann Surg Oncol 2017,24:2174-81.
11. Kitajima K, Fukushima K, Miyoshi Y, Katsuura T, Iqarashi Y, Kawanaka Y, Mouri M, Maruyama K, Yamano T, Doi H, Yamakado K, HirotaS,Hirota S. Diagnostic and prognostic value of (18)F-FDG PET/CT for axillary lymph node staging in patients with breast cancer. Jpn J Radiol 2016;34:220-8.
12. Seo MJ, Lee JJ, Kim HO,Chae SY, Park SH, Ryu JS,Ahn SH, Lee JW, Son BH, Gong GY, Moon DH. Detection of internal mammary lymph node metastasis with (18) F-fluorodeoxyglucose positron emission tomography/ computed tomography in patients with stage III breast cancer. European Journal of Nuclear Medicine and Molecular Imaging 2014;41:438-45
13. Chen Z, Yang J, Li S, Lv M, Shen Y, Wang B, Li P, Yi M, Zhao X, Zhang L, Wang L,YangJ.Invasive lobular carcinoma of the breast: A special histological type compared with invasiveductal carcinoma. PLoS One 2017;12:e0182397.
14. Liu Q, Xiang HY, Ye JM, Xu L, Zhang H, Zhang S, Duan XN, Liu Yh. An analysis of 68 invasive lobular breast cancer cases in clinicopathological characteristics and the prognostic determinants. Zhonghua Wai Ke Za Zhi 2018;56:119-23.
15. Kim I , Choi HJ, Ryu JM, Lee SK,Yu JH, Kim SW, Nam SJ, Lee JE. Prognostic Validation of the American Joint Committee on Cancer 8th Staging System in 24,014 Korean Patients with Breast Cancer. J Breast Cancer 2018;21:173-81.
16. An YS, Lee DH, Yoon JK, Lee SJ, Kim TH, Kang DK, Kim KS, Jung YS, Yim H. Diagnostic performance of 18F-FDG PET/CT, ultrasonography and MRI. Detection of axillary lymph node metastasis in breast cancer patients. Nuklearmedizin 2014;53:89-94.
17. Zhang X, Zheng C, Yang Z, Cheng Z, Deng H, Chen M, Duan X, Mao J,Shen J. Axillary Sentinel Lymph Nodes in Breast Cancer: Quantitative Evaluation at Dual-Energy CT. Radiology 2018;289:337-346.
18. Thakur SB, Durando M, Milans S, Cho GY, Gennaro L, Sutton EJ, Giri D, Morris EA Apparent diffusion coefficient in estrogen receptor-positive and lymph node-negative invasive breast cancers at 3.0T DW-MRI: A potential predictor for an oncotype Dx test recurrence score. J Magn Reson Imaging 2018,47:401-9.
19. Taira N, Ohsumi S, Takabatake D, Hara F, Takashima S, Aogi K, Takashima S, Inoue T, Sugata S, Nishimura R. Determination of indication for sentinel lymph node biopsy in clinical node-negative breast cancer using preperative18F-fluorodeoxyglucose positron emission tomography/computed tomography fusion imaging. Jpn J Clin Oncol 2009;39:16-21.
20. Yoo J, Kim BS, Yoon HJ. Predictive value of primary tumor parameters using 18F-FDG PET/CT for occult lymph node metastasis in breast cancer with clinically negative axillary lymph node. Ann Nucl Med 2018;32:642-8.
21. Evangelista L, Cervino AR, Michieletto S,Saibene T, Orvieto E, Bozza F, Ghiotto C. Staging of locally advanced breast cancer and the prediction of response to neoadjuvant chemotherapy: complementary role of scintimammography and 18F-FDG PET/CT. Q J Nucl Med Mol Imaging 2017;61:205-15.
22. Riedl CC, Pinker K, Ulaner GA, Ong LT, Baltzer P, Jochelson MS, McArthur HL, Gonen M, Dickler M, Weber WA. Comparison of FDG-PET/CT and contrast-enhanced CT for monitoring therapy response in patients with metastatic breast cancer. Eur J Nucl Med Mol Imaging 2017,44:1428-37.
23. Brito AE, Santos A, Sasse AD, Cabello C, Oliveira P, Mosci C, Souza T, Amorim B, Lima M, Ramos CD, Etchebehere E. 18F-Fluoride PET/CT tumor burden quantification predicts survival in breast cancer. Oncotarget 2017;8:36001-11.
24. Paydary K, Seraj SM, Zadeh MZ, Emamzadehfard S, Shamchi SP, GholamiS,Werner TJ, Alavi A. The Evolving Role of FDG-PET/CT in the Diagnosis, Staging, and Treatment of Breast Cancer. Mol Imaging Biol 2019;21:1-10.
25. Kawada N, Uehara H, Hosoki T, Takami M, Shiroeda H, Arisawa T, Tomita Y. Usefulness of dual-phase 18F-FDG PET/CT for diagnosing small pancreatic tumors. Pancreas 2015;44:655-9.
26. Zhuang H, Pourdehnad M, Lambright ES, Yamamoto AJ, Lanuti M, Li P, Mozley PD, Rossman MD, Albelda SM, Alavi A. Dual time point18F-FDG PET imaging for differentiating malignant from inflammatory processes. J Nucl Med 2001;42:1412-7.
27. Delbeke D, Coleman RE, Guiberteau MJ, Brown ML, Royal HD, Siegel BA, Townsend DW, Berland LL, Parker JA, Hubner K, Stabin MG, Zubal G, Kachelriess M, Cronin V, Holbrook S. Procedure guideline for

tumor imaging with 18F-FDG PET/CT 1.0. J Nucl Med 2006;47:885-95.
28. Lee JK, Min KJ, So KA, Kim S, Hong JH. The effectiveness of dual-phase 18F-FDG PET/CT in the detection of epithelial ovarian carcinoma: a pilot study. J Ovarian Res 2014;7:15.
29. Costantini DL, Vali R, Chan J, McQuattie S, Charron M. Dual-time-point FDG PET/CT for the evaluation of pediatric tumors. AJR Am J Roentgenol 2013;200:408-13.
30. Razak HR, Geso M, Abdul Rahim N, Nordin AJ. Imaging characteristics of extrapulmonary tuberculosis lesions on dual time point imaging (DTPI) of FDG PET/CT. J Med Imaging Radiat Oncol 2011;55:556-62.
31. Jung NY, Kim SH, Kim SH, Seo YY, Oh JK, Choi HS, You WJ. Effectiveness of Breast MRI and 18F-FDG PET/CT for the Preoperative Staging of Invasive Lobular Carcinoma versus Ductal Carcinomal. J Breast Cancer 2015;18:63-72.
32. An YS, Kang DK, Jung Y, Kim TH. Volume-based metabolic parameter of breast cancer on preoperative 18F-FDG PET/CT could predict axillary lymph node metastasis. Medicine (Baltimore) 2017;96:e8557.
33. Lee JW, Kim EY, Kim DJ, Lee JH, Kang WJ, Lee JD, Yun M. The diagnostic ability of (18)F-FDG PET/CT for mediastinal lymph node staging using (18)F-FDG uptake andvolumetric CT histogram analysis in non-small cell lung cancer. Eur Radiol 2016;26:4515-23.
34. Yuan SH, Yu JM, Yu YH, Fu Z, Guo HB, Liu TH, Yang XH, Yang GR, Li WW. FDG PET/CT versus PET alonefor presurgical detection of lymph node metastasis in esophageal carcinoma. Zhonghua Zhong Liu Za Zhi 2007;29:221-4.
35. Cheng G, Torigian DA, Zhuang H, Alavi A. When should we recommend use of dual time-point and delayed timepoint imaging techniques in FDG PET? Eur J Nucl Med Mol Imaging 2013;40:779-787.
36. Matthiessen LW, Johannesen HH, Skougaard K, Gehl J, Hendel HW. Dual time point imaging fluorine-18 flourodeoxyglucose positron emission tomography for evaluation of large loco-regional recurrences of breast cancer treated with electrochemotherapy. Radiol Oncol 2013;47:358-365.
37. Ma J, Liu L, Tang L, Zong J, Lin A, Lu T, Cui C, Li L. Retropharyngeal lymph node metastasis in nasopharyngeal carcinoma: prognostic value and staging categories. Clin Cancer Res 2007;13:1445-52.
38. Yu L, Tian M, Gao X, Wang D, Qin Y, Geng J. The method and efficacy of 18F-fluorodeoxyglucose positron emission tomography/computedtomography for diagnosing thelymphatic metastasis of colorectal carcinoma. Acad Radiol 2012;19:427-33.

Cite this article as: Zhang J, Shi X, Xiao Y, Ma C, Cao G, Liu Y, Li Y. Early SUVmax is the best predictor of axillary lymph node metastasis in stage III breast cancers. Quant Imaging Med Surg 2021;11(5):1680-1691. doi: 10.21037/qims-20-423

Supplementary

Table S1 Clinical characteristics of 40 patients

Number	Age	Tumor site	Pathological types	Tumor diameter	Total number of lymph nodes		Lymph nodes matched with PET/CT	
					Metastatic	Non-metastatic	Metastatic	Non-metastatic
1	72	Right	Ductal	2.4	4	7	2	3
2	71	Left	Ductal	5.7	4	8	3	4
3	70	Right	Ductal	3.1	7	7	1	2
4	69	Left	Lobular	2.9	5	4	2	2
5	68	Right	Lobular	3.1	4	7	2	4
6	67	Left	Ductal	1.3	7	6	3	3
7	66	Right	Ductal	2.6	4	5	2	2
8	65	Left	Lobular	1.8	4	6	3	4
9	65	Left	Ductal	1.1	4	5	4	4
10	64	Right	Lobular	2.8	5	6	1	2
11	64	Left	Ductal	4.1	4	7	2	3
12	63	Right	Ductal	3.2	4	4	2	2
13	62	Left	Ductal	2.5	4	5	2	3
14	62	Right	Ductal	1.5	4	7	2	4
15	61	Right	Lobular	1.3	4	6	3	3
16	60	Left	Lobular	2.3	4	4	1	2
17	59	Left	Ductal	3.3	4	8	2	5
18	58	Right	Ductal	3.7	4	8	3	3
19	57	Right	Ductal	2.9	4	6	2	3
20	56	Left	Lobular	3.4	8	5	4	3
21	56	Left	Ductal	2.7	4	7	1	2
22	55	Right	Ductal	1.7	4	6	2	3
23	54	Left	Ductal	2.1	4	4	3	2
24	54	Right	Ductal	3.4	4	8	2	5
25	53	Left	Ductal	1.2	4	3	3	2
26	52	Left	Ductal	1.6	4	5	2	2
27	52	Left	Ductal	4.1	6	6	3	3
28	52	Right	Ductal	2.8	4	5	3	3
29	51	Left	Lobular	2.2	4	4	2	3
30	51	Left	Ductal	1.9	4	7	3	2
31	50	Right	Ductal	1.1	4	4	2	2
32	48	Right	Lobular	3.2	4	6	2	2
33	47	Left	Ductal	2.5	4	4	3	2
34	44	Right	Ductal	2.3	5	5	4	4
35	41	Left	Ductal	4.1	4	7	2	3
36	40	Left	Ductal	0.8	4	3	2	1
37	39	Right	Ductal	1.7	4	5	2	2
38	37	Right	Ductal	3.5	5	4	3	2
39	36	Left	Ductal	2.1	4	5	4	4
40	33	Left	Ductal	3.1	4	3	3	2

http://dx.doi.org/10.21037/qims-20-423